UMN–TH–4004/20
FTPI–MINN–20/35
November 2020

The Impact of New $d(p,\gamma)^3\mathrm{He}$ Rates on Big Bang Nucleosynthesis

Tsung-Han Yeh
Department of Physics, University of Illinois, Urbana, IL 61801

Keith A. Olive
William I. Fine Theoretical Physics Institute, School of Physics and Astronomy, University of Minnesota, Minneapolis, MN 55455, USA

Brian D. Fields
Departments of Astronomy and of Physics, University of Illinois, Urbana, IL 61801

arXiv:2011.13874v1 [astro-ph.CO] 27 Nov 2020

Abstract

We consider the effect on Big Bang Nucleosynthesis (BBN) of new measurements of the $d(p,\gamma)^3$He cross section by the LUNA Collaboration. These have an important effect on the primordial abundance of D/H which is also sensitive to the baryon density at the time of BBN. We have re-evaluated the thermal rate for this reaction, using a world average of cross section data, which we describe with model-independent polynomials; our results are in good agreement with a similar analysis by LUNA. We then perform a full likelihood analysis combining BBN and *Planck* cosmic microwave background (CMB) likelihood chains using the new rate combined with previous measurements and compare with the results using previous rates. Concordance between BBN and CMB measurements of the anisotropy spectrum using the old rates was excellent. The predicted deuterium abundance at the Planck value of the baryon density was $(\mathrm{D/H})^{\mathrm{old}}_{\mathrm{BBN+CMB}} = (2.57\pm0.13)\times10^{-5}$ which can be compared with the value determined from quasar absorption systems $(\mathrm{D/H})_{\mathrm{obs}} = (2.55 \pm 0.03) \times 10^{-5}$. Using the new rates we find $(\mathrm{D/H})_{\mathrm{BBN+CMB}} = (2.51 \pm 0.11) \times 10^{-5}$. We thus find consistency among BBN theory, deuterium and ^{4}He observations, and the CMB, when using reaction rates fit in our data-driven approach. We also find that the new reaction data tightens the constraints on the number of relativistic degrees of freedom during BBN, giving the effective number of light neutrino species $N_\nu = 2.880\pm0.144$ in good agreement with the Standard Model of particle physics. Finally, we note that the observed deuterium abundance continues to be more precise than the BBN+CMB prediction, whose error budget is now dominated by $d(d,n)^3$He and $d(d,p)^3$H. More broadly, it is clear that the details of the treatment of nuclear reactions and their uncertainty have become critical for BBN.

I. INTRODUCTION

Big Bang Nucleosynthesis (BBN) is one of the deepest probes in the early universe which uses known physics [1–19]. Standard BBN is formulated in the context of a ΛCDM cosmology, standard nuclear and particle physics with three light neutrino flavors. Given the reasonably accurate value of the neutron mean-life, $\tau_n = 879.4 \pm 0.6$ s [20], and the determination of the baryon density, $\omega_B = \Omega_B h^2$, (or baryon-to-photon ratio, $\eta = n_{\rm B}/n_\gamma$) from the cosmic microwave background (CMB) anisotropy spectrum [21], BBN is effectively a parameter-free theory [5]. The theory predicts the primordial abundances of the light element isotopes, D, ^{3}He, ^{4}He, and ^{7}Li. While there is no direct comparison to an observation of primordial ^{3}He, the other three isotopes can be tested by observations. Despite the well known discrepancy[1] with ^{7}Li [14, 28], both ^{4}He and D are in excellent agreement with observations.

Rather than simply computing the light elements abundances assuming a particular value of η quoted by Planck, we have, in previous work [18, 19], advocated a likelihood approach which convolves the Planck likelihood chains, with a Monte-Carlo simulation of nuclear cross sections. In [19], hereafter FOYY, the combined BBN+CMB likelihood functions for ^{4}He and D/H are characterized by a mean and width given by $Y_p = 0.2469 \pm 0.0002$ and D/H $\times 10^5 = 2.57 \pm 0.13$ where Y_p is the primordial ^{4}He mass fraction, and D/H is the abundance of deuterium by number relative to hydrogen. These should be compared with the observational determinations, $Y_p = 0.2453 \pm 0.0034$ [29] [2] and

$$({\rm D/H})_{\rm obs} = (2.55 \pm 0.03) \times 10^{-5} \tag{1}$$

based on an weighted average of 11 measurements [31–38]. As one can see, both observations are in excellent agreement with BBN predictions.

The BBN predictions of the light element abundances rely on a detailed network of nuclear reaction rates, thermally averaged over the energy range of importance to BBN. Each of the these rates carries an uncertainty, which is used in a Monte-Carlo simulation to produce likelihood distributions of each of the light element abundances. Clearly accurate measurement of nuclear cross sections are critical for obtaining accurate light element abundances.

[1] It is quite unlikely [22–25] that the solution to the lithium problem resides in the underlying nuclear physics. The discrepancy may be a result of stellar depletion [26] and there is some evidence of a broken lithium plateau at very low metallicity [27]. We do not consider the lithium problem further here.

[2] This value is an update of the value used in FOYY, $Y_p = 0.2449 \pm 0.0040$ [30].

Indeed, the deuterium observational error budget is far tighter than the 5% level found when combining BBN theory (pre-LUNA) and the CMB [19].

Among the processes of particular importance for calculating the D/H abundance is $d(p,\gamma)^3$He. Our nominal rate for this process is based on an average of several experimental measurements compiled by NACRE [39] in the energy range of interest to BBN. Nollett and collaborators have emphasized [35, 40, 41] that theoretical calculations predict a cross section 20% larger than the measurements in the BBN energy range. These calculations are derived from an *ab initio* quantum mechanical calculation using nucleon interaction potentials, and agree with $d(p,\gamma)^3$He data at energies outside of the BBN window. An independent calculation by Marcucci and collaborators [42], updated in [43], finds a similar mismatch at BBN energies. Another theory-based approach is the R-matrix analysis was used by the Paris group [16]. This also gives a higher BBN cross section and rate. The higher rate leads to a lower abundance of D/H, and a primordial value of D/H $\times 10^5 = 2.45 \pm 0.05$ was found [16], updated to D/H $\times 10^5 = 2.46 \pm 0.04$ [17], both in evident disagreement with observations.

Thus it has become clear that new, precision $d(p,\gamma)^3$He data is needed, at energies targeted for BBN. As a result, dedicated experiments have been conducted. Ref. [44] first presented new results in the BBN energy range, finding cross sections between the older data and the theoretical predictions. These used a thick-target method, with an error budget somewhat larger than the older data. Meanwhile, an intensive study was initiated at the Laboratory for Underground Nuclear Astrophysics (LUNA) in the Gran Sasso National Laboratory [45]. Commissioning of the LUNA $d(p,\gamma)^3$He experiment was described in [46] and results have now been released [47]. As we will see in more detail, the new LUNA data cover the entire BBN energy range with good sampling. Just as importantly, they feature a tight systematic and statistical error budget. The measured LUNA cross section shows a slight increase compared to earlier measurements in the BBN energy range, but remains significantly below the theoretical calculations. This long-anticipated result marks a major advance in understanding this rate and indeed all of BBN, and motivates our study here.

In this note, we first include in section II the newly measured $d(p,\gamma)^3$He to update the results of FOYY. In section III, we compare the our previous results, with those replacing the $d(p,\gamma)^3$He rate with the new experimental result [47] as well as our new baseline result based on averaging the new measurement with existing cross section measurements. We

also compare these results with the calculated abundances using the theoretical rate for $d(p,\gamma)^3$He [43]. We find that the world averaged cross-section is only slightly reduced relative to the new measurement, but the uncertainty is substantially reduced due to the significant improvement of the measurement precision [47]. While we find that the BBN-CMB predicted value for D/H is decreased to $(2.51 \pm 0.11) \times 10^{-5}$, it remains consistent with observations and remains significantly larger than the result based on the theoretical cross section which yields $(2.42 \pm 0.10) \times 10^{-5}$. We also discuss in section IV the results when the number of neutrino degrees of freedom, N_ν, is not held fixed at 3. We summarize the impact of our results in section V.

II. THE $d(p,\gamma)^3$He CROSS SECTION AND RATE

We have performed a new calculation of the $d(p,\gamma)^3$He thermonuclear rate and its uncertainty. To do this, we first evaluate the $d(p,\gamma)^3$He cross section. We use cross section data from LUNA [46, 47], as well as earlier work from 1997 by Schmid et al. [48] and Ma et al. [49], and from the 1960s by Wölfli et al. [50] and Griffiths et al. [51].[3] These data are plotted in Fig. 1 in terms of the astrophysical $S(E) = E\ \sigma(E)\ e^{2\pi\eta_s}$ where for this reaction the usual barrier penetration exponent is $2\pi\eta_s = 2\pi e^2/\hbar v$, with $v(E)$ the relative velocity. We see that the S-factor is a smooth function of energy, and nearly linear in the BBN energy range.

Following a procedure similar to Cyburt [9] and FOYY, we perform a global fit for $S(E)$ over the energy range 2 keV to 2 MeV, which encompasses the BBN range. We describe $S(E)$ with a polynomial in E, and we find that a 3rd-order expansion is sufficient to characterize the rate without overfitting. We combine the statistical and systematic errors in quadrature to obtain and energy-dependent error, and use it to find a global best fit and associated uncertainty band arising from minimizing χ^2. This amounts to a weighted average favoring measurements like LUNA with small statistical and systematic errors. We include an energy-independent discrepancy error based that accounts for systematic differences between data sets; this amounts to requiring an overall χ^2 per degree of freedom no larger than unity.

For comparison, in FOYY we used NACRE-II [39] for this reaction; their global fit of

[3] We do not use the results of refs. [52] nor [53] due to systematic issues with the stopping powers they used, as pointed out by both Ma [49] and Schmid [48].

course did not include LUNA, but also used a larger data set that extended to higher energies far outside of the BBN range. LUNA performed their own global fit, using a polynomial-based procedure very similar to ours. Finally, the theory-based *ab initio* predictions of [43] do not directly use $d(p,\gamma)^3$He but do include an error analysis based on the uncertainties in the model inputs; in using their result we combine their two error terms in quadrature.

Figure 1 shows the astrophysical S-factor for $d(p,\gamma)^3$He with the measurements and fits considered in this work, plotted as a function of energy displayed on a linear scale (left) and an expanded log scale (right). The curves show the fits we considered, corresponding to 1) the NACRE-II [39] S-factor used in FOYY (blue dotted); 2) the theoretical S-factor [43] (green dot-dashed); 3) the LUNA global average [47] (red dashed); and 4) our newly world average rate (black solid). As one can see, our world averaged result (which we take to be our current baseline) is very similar to the new LUNA measurement and lies between the NACRE-II average and the theoretical calculation (though the new result is much closer to the former).

For each set of $S(E)$ factors shown in Fig. 1, we compute a thermal average in the usual manner to obtain a thermonuclear rate coefficient as a function of temperature:

$$\lambda(T) = N_{\rm Avo}\langle\sigma v\rangle = m_{\rm u}^{-1}\left(\frac{8}{\mu\pi}\right)^{1/2}(kT)^{-3/2}\int_{E_{\rm min}}^{E_{\rm max}} S(E)\; e^{-2\pi\eta}\; e^{-E/kT}\; dE \qquad (2)$$

where Avogadro's number $N_{\rm Avo} = 1/m_{\rm u}$ is also the inverse of the atomic mass unit $m_{\rm u}$, and μ is the reduced mass. We choose integration limits $(E_{\rm min}, E_{\rm max}) = (0, 100T)$.

The relative difference between the thermonuclear rates is shown in Fig. 2. We set our baseline average (corresponding to the black solid curve in Fig. 1) to 1 and display the other three rates relative to this. We see that compared to the rate used in FOYY based on the NACRE-II S-factor, the rate has increased at all temperatures in the BBN range, with about a 6.5% increase around $T = 10^9$ K where the rate is most important. On the other hand, our rate remains $\sim 10\%$ lower than the theoretical prediction. Finally, our results are quite similar to the LUNA global average, reflecting our similar approaches, and indeed they are almost identical around and below the $T = 10^9$ K regime important for BBN.

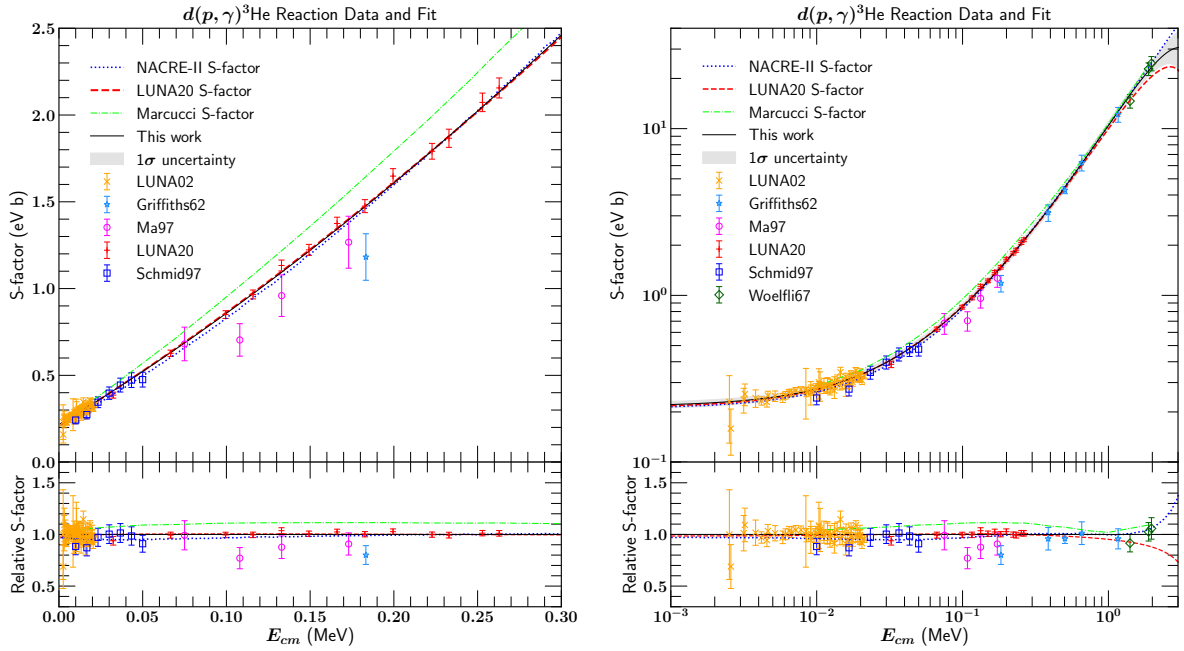


FIG. 1. The astrophysical S-factor for $d(p,\gamma)^3$He showing 1) the NACRE-II [39] S-factor used in FOYY (blue dotted); 2) the theoretical S-factor [43] (green dot-dashed); 3) the LUNA global average [47] (red dashed); and 4) our new world average rate (black solid). The shading corresponds to the 68% uncertainty we assign to the average rate. In the left panel, the S-factor is shown against a linear energy scale centered on the BBN energies. In the right panel, we show an extended energy range on a log scale.

III. RESULTS FOR FIXED $N_\nu = 3$

To describe the impact of the newly measured $d(p,\gamma)^3$He cross section, we first briefly review our method for constructing BBN likelihood functions. As uncertainties in the input BBN reactions play a pivotal role in determining the uncertainties in the light element abundances, we apply Monte-Carlo techniques [54–57] for constructing likelihood functions. These have been discussed in detail in [18, 19], so here we summarize briefly.

We generate likelihoods for BBN light element predictions via a Monte Carlo approach. For the case of $N_\nu = 3$ we run our BBN code for a grid in η; when N_ν is allowed to vary we run for a grid in (η, N_ν). For each grid point, i.e., each value of η and N_ν, we run the BBN code 10000 times allowing the key nuclear rates to vary according to their uncertainties. Each rate is drawn from a Gaussian distribution with the appropriate mean and uncertainty.

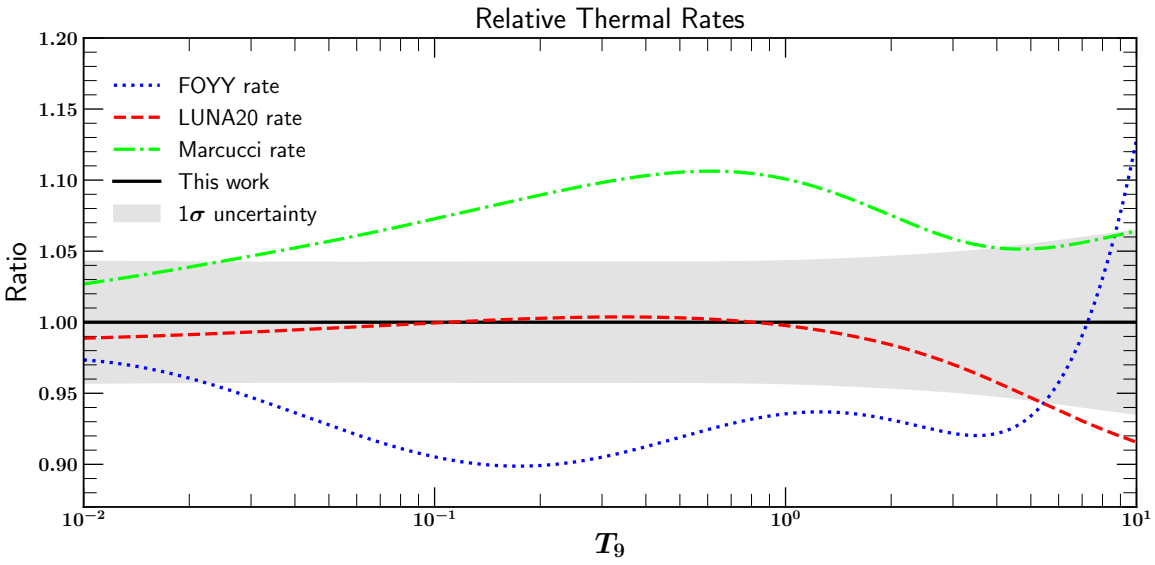


FIG. 2. The relative difference between the rates compared to our new baseline average. Shown here as a function of temperature in units of 10^9 K.

From the resulting light element abundances at each (η, N_ν) grid point we compute the mean and uncertainties. From these we infer BBN likelihood functions for the entire grid. In the case of fixed $N_\nu = 3$, this gives $\mathcal{L}_{\rm BBN}(\eta; X)$ with abundances $X \in (Y_p, {\rm D/H})$, and for N_ν varying we compute $\mathcal{L}_{\rm NBBN}(\eta, N_\nu; X)$.

The CMB independently measures η to an exquisite precision, and now also provides important constraints on Y_p and N_ν. As noted above, we define a CMB likelihood function, derived from the Markov chains generated from the final *Planck* 2018 data release [21].[4] As in FOYY, we use the CMB chains based on temperature and polarization data, TT+TE+EE+lowE, including CMB lensing. The chains we employ do not assume any BBN relation between the baryon density and helium abundance. We separately consider the cases where $N_\nu = 3$ is fixed, and where it is free to vary; the resulting likelihoods are called $\mathcal{L}_{\rm CMB}(\eta, Y_p)$ and $\mathcal{L}_{\rm NCMB}(\eta, Y_p, N_\nu)$ respectively. These can be convolved with the BBN likelihood functions defined above. In addition, we have the observational likelihoods $\mathcal{L}_{\rm Obs}(X)$ which are assumed to be Gaussians based on the observational determinations for $X \in (Y_p, {\rm D/H})$.

We begin with the construction of the BBN-CMB likelihood functions for the light element

[4] We use the `base_yhe` and `base_nnu_yhe` chains in https://wiki.cosmos.esa.int/planck-legacy-archive/index.php/Cosmological_Parameters

abundances. For now, we will assume $N_\nu = 3$ and consider the more general case below. The combined likelihood is defined by

$$\mathcal{L}_{\rm BBN+CMB}(X_i) \propto \int \mathcal{L}_{\rm CMB}(\eta, Y_p)\ \mathcal{L}_{\rm BBN}(\eta; X_i)\ d\eta\,, \tag{3}$$

where we normalize each of the likelihood functions so that at their peaks $\mathcal{L} = 1$.

We show in Fig. 3 the D/H likelihood as defined in Eq. (3) using four choices of the rate for $d(p,\gamma)^3$He and shown in Fig. 1 : i) the rate used in FOYY (upper left), ii) the theoretical rate suggested in [43] (upper right), iii) the newly measured rate from [47] (lower left), and iv) our new combined rate including the results of [47] (lower right). The combined BBN+CMB likelihood from Eq. (3) is shaded purple. The observational likelihood is shaded yellow. As we have claimed previously [18, 19], when using the FOYY rate for $d(p,\gamma)^3$He , we get near perfect agreement between the BBN-CMB calculated deuterium abundance ($(2.574 \pm 0.129) \times 10^{-5}$) and the observational determination (eq. 1) as seen in the upper left panel. In contrast, using the theoretical rate [43] gives a mean abundance of $(2.417 \pm 0.103) \times 10^{-5}$ and leads to a shift to the left of the theoretical likelihood (purple). Using either the LUNA rate [47], or our averaged rate gives a virtually identical result, $(2.503 \pm 0.106) \times 10^{-5}$ and $(2.506 \pm 0.110) \times 10^{-5}$ as seen in the lower panels of Fig. 3. These remain in excellent agreement with observations.

The BBN+CMB likelihoods in Fig. 3 are summarized by the predicted abundances for D/H given in Table I, where the central values give the mean, and the error gives the 1σ variance. The third column gives the value at the peak of the distribution. Each of these results can be compared to the observed abundance in eq. (1).

TABLE I. The mean and peak values of D/H for each of the adopted rates for $d(p,\gamma)^3$He .

$d(p,\gamma)^3$He rate	mean D/H $\times 10^5$	peak D/H $\times 10^5$
FOYY [19]	2.574 ± 0.129	2.572
Theory [43]	2.417 ± 0.103	2.416
LUNA20 [47]	2.503 ± 0.106	2.502
This Work	2.506 ± 0.110	2.504

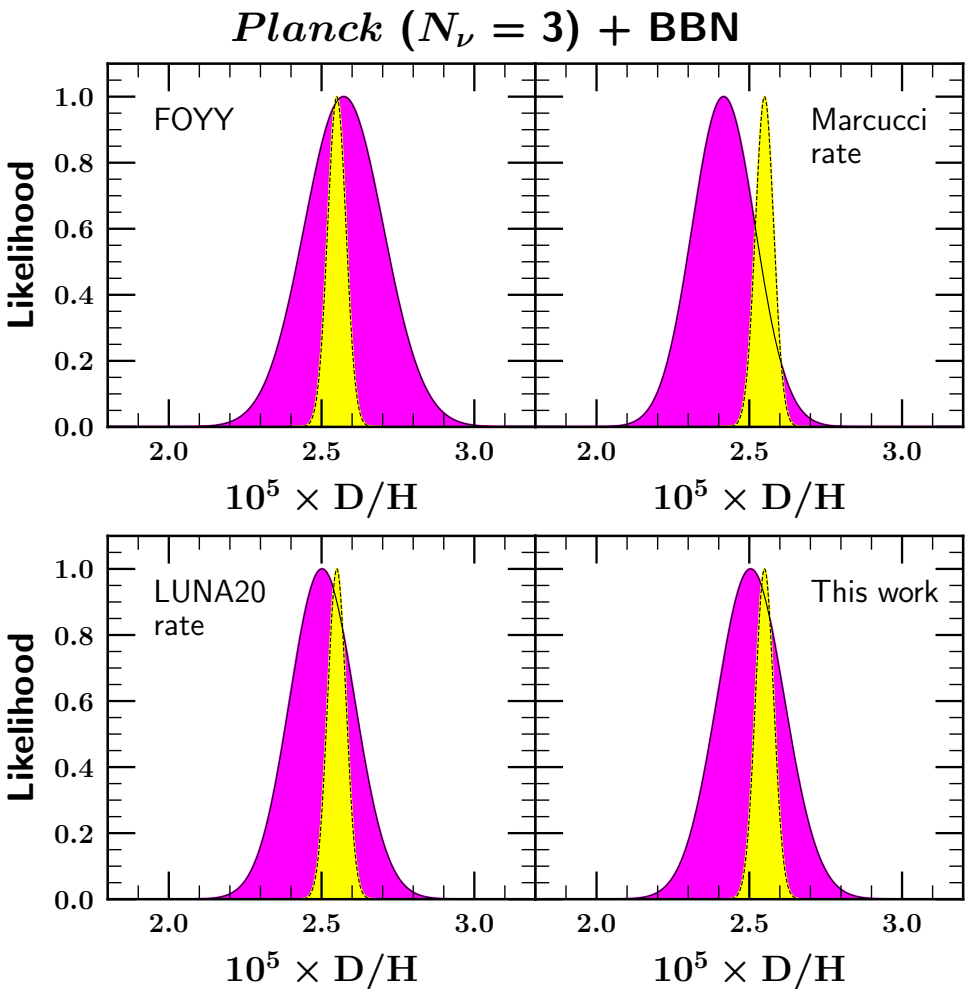


FIG. 3. Likelihood functions for D/H with different assumed rates for $d(p,\gamma)^3$He : i) the FOYY rate (upper left), ii) the theoretical rate suggested in [43] (upper right), iii) the newly measured rate from [47] (lower left), and iv) our new combined rate including the results of [47] (lower right). The solid-lined, dark-shaded (purple) curves are the BBN+CMB predictions, based on *Planck* inputs as discussed in the text. The dashed-lined, light-shaded (yellow) curves show measurements from quasar absorption systems.

The relative change in D/H is shown in Fig. 4 as a function of η. The D/H abundance using our current averaged rate is set at 1 and the reductions or enhancement in D/H for the other three rates are shown as labelled. Once again, we see the very small difference in the resulting D/H between the rate calculated here, and the one provided by LUNA [47].

As the $d(p,\gamma)^3$He rate also affects ^{4}He and ^{7}Li, we show in Fig. 5 the likelihood functions

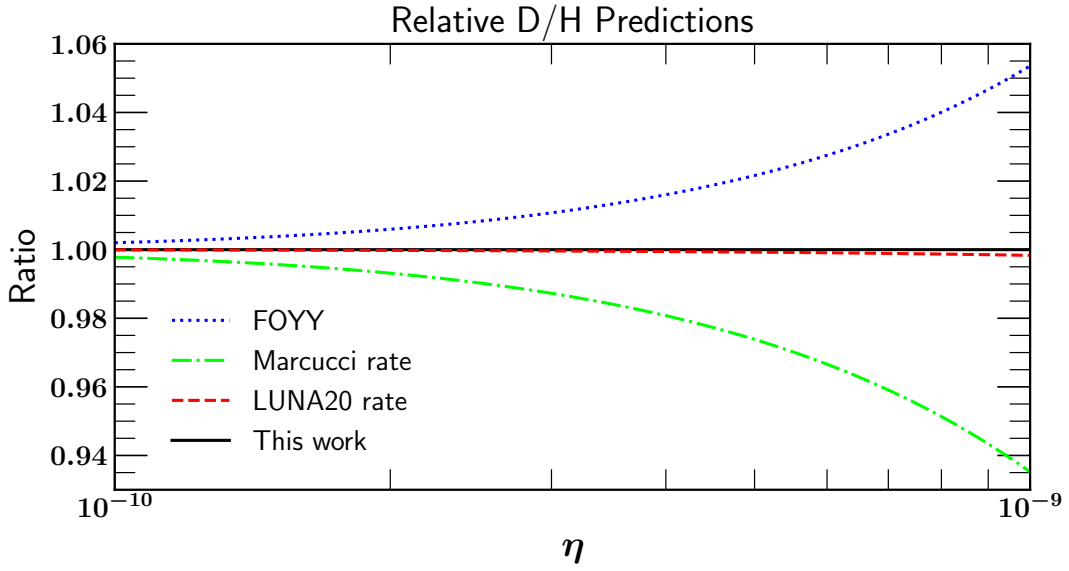


FIG. 4. The relative change in the D/H abundance using our previous (FOYY) rate as a function of η.

for ^{4}He (upper panels) and ^{7}Li (lower panels), comparing the previous results from FOYY (left panels) with the combined results which include the newly measured $d(p,\gamma)^3$He rate (right panels). In the case of ^{4}He, we also show the likelihood obtained by integrating $\mathcal{L}_{\rm CMB}(\eta, Y_p)$ over η corresponding to the Planck CMB determination of Y_p. As one might expect, there is virtually no change in the helium abundance. In contrast there is a more noticeable change in Li/H towards higher values, thus worsening the lithium problem (slightly).

The predicted abundances for ^{4}He and ^{7}Li from Fig. 5 in addition to the remaining two rates are summarized in Table II.

We can marginalize any of our likelihood functions to obtain a likelihood as a function of η alone, $\mathcal{L}(\eta)$. We note that the CMB-alone value for $\eta_{10} = \eta \times 10^{10}$ is relatively low, 6.104 ± 0.058 [19]. When the BBN relation between Y_p and η is included, the best fit value for η_{10} is higher, 6.129 ± 0.040. Although D/H is commonly referred to as an excellent baryometer, the still relatively large uncertainty in the calculated D/H abundance does not affect the likelihood in a significant way. From the upper left panel of Fig. 3, we see that the observed D/H abundance is lower than the calculated value and should draw the best

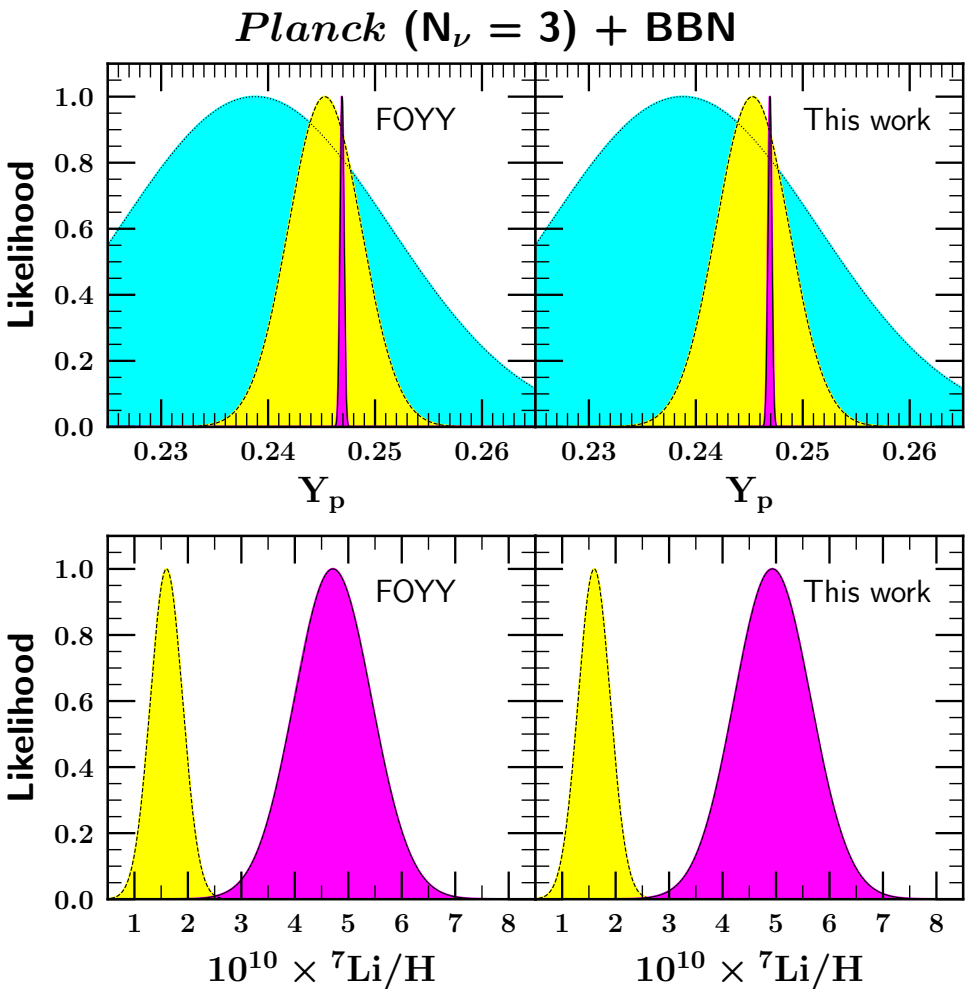


FIG. 5. Likelihood functions for ^{4}He (upper panels) and ^{7}Li (lower panels). Here we consider only the FOYY $d(p,\gamma)^3$He rate (left panels) and our new combined rate including the results of [47] (right panels) The solid-lined, dark-shaded (purple) curves are the BBN+CMB predictions, based on *Planck* inputs as discussed in the text. The dashed-lined, light-shaded (yellow) curves show the observational likelihood functions. For ^{4}He, the dotted-lined, medium- shaded (cyan) curve shows the independent CMB determination of ^{4}He.

fit value of η_{10} upwards. It does, but only marginally so, and within round-off it remains at 6.129 ± 0.040.

This behavior (or lack thereof) can be understood by the likelihood functions shown in Fig. 6. Here we show projections of the likelihood functions onto the (Y_p, η_{10}) plane. The tilted blue ellipses in the left panel show the 68.3%, 95.4%, and 99.7% confidence level contours for the the CMB-alone likelihood function, $\mathcal{L}_{\rm CMB}(\eta, Y_p)$. This is centered on

TABLE II. The mean and peak values of Y_p and Li/H for each of the adopted rates for $d(p,\gamma)^3$He .

$d(p,\gamma)^3$He rate	mean Y_p	peak Y_p
FOYY [19]	0.24691 ± 0.00018	0.24691
Theory [43]	0.24693 ± 0.00018	0.24693
LUNA20 [47]	0.24693 ± 0.00018	0.24693
This Work	0.24693 ± 0.00018	0.24693
$d(p,\gamma)^3$He rate	mean Li/H $\times 10^{10}$	peak Li/H $\times 10^{10}$
FOYY [19]	4.72 ± 0.72	4.71
Theory [43]	5.26 ± 0.75	5.26
LUNA20 [47]	4.94 ± 0.71	4.94
This Work	4.94 ± 0.72	4.93

$\eta_{10} = 6.104$. Ignoring the CMB, we show the convolved BBN+Obs likelihood by the set of cyan ellipses. These are more easily seen in the zoomed-in version shown in the right panel. Despite the precision in the observed D/H abundance, the mean value for η_{10} found from this likelihood function is 6.143 ± 0.190 [19]. Thus the observed abundance, which for the FOYY $d(p,\gamma)^3$He rate is lower than the calculated abundance, tries to drive the value of η up, when combined with the CMB. However the large uncertainty in η in the BBN+Obs likelihood means that the pull is very weak. Indeed, for CMB+BBN+Obs the mean value in η_{10} remains essentially the same at 6.129, shifting by < 0.001.

We show in Fig. 7, a similar projection of the likelihood functions when using the newly averaged $d(p,\gamma)^3$He rate which includes the LUNA measurement [47]. As one can see, the BBN+Obs ellipses remain elongated due to the residual uncertainty in the rates which determine D/H. In addition we see that they are shifted to lower values of η. Indeed, these are are now centered around $\eta_{10} = 6.04$ below both the CMB and BBN+CMB likelihoods. Nevertheless, the because of the relatively large uncertainty in η, the combined likelihood, while shifted to lower values of η_{10}, shifts only to 6.123 (from 6.129).

Our total combined likelihood distribution marginalized to give a function of η can be

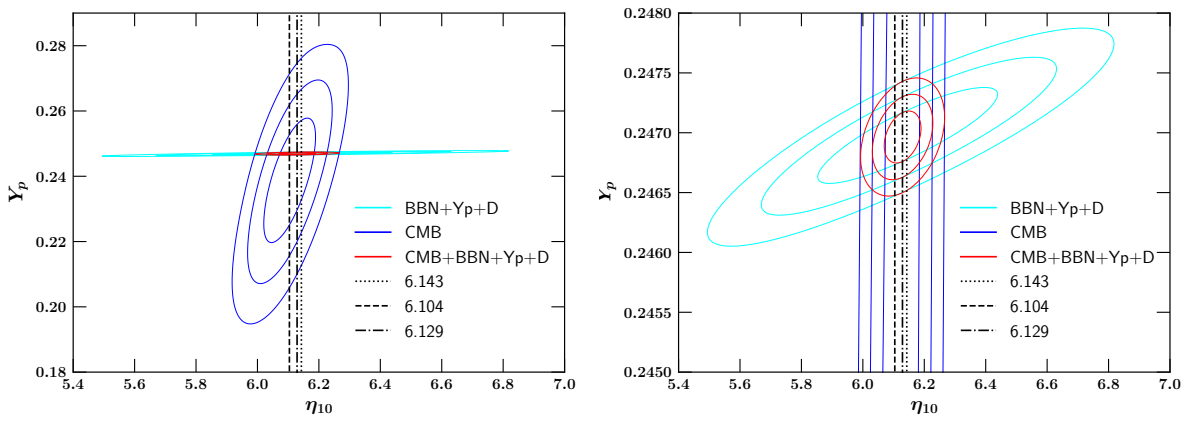


FIG. 6. Likelihood functions using the FOYY $d(p,\gamma)^3$He rate projected onto the (η_{10}, Y_p) plane. The right panel focuses on a more narrow range of values of Y_p.

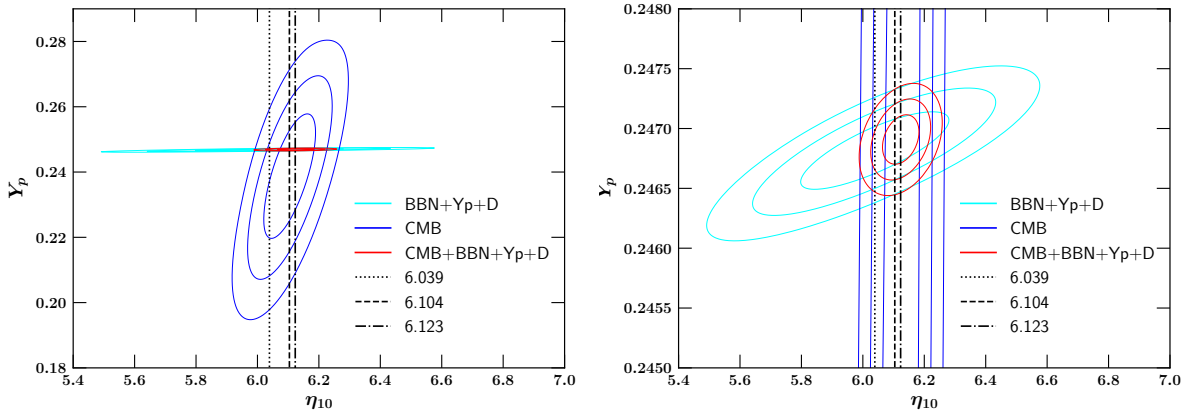


FIG. 7. Likelihood functions using our new averaged $d(p,\gamma)^3$He rate projected onto the (η_{10}, Y_p) plane. The right panel focuses on a more narrow range of values of Y_p.

expressed as

$$\mathcal{L}_{\rm BBN+CMB+Obs}(\eta) \propto \int \mathcal{L}_{\rm CMB}(\eta, Y_p)\mathcal{L}_{\rm BBN}(\eta; X_i)\ \mathcal{L}_{\rm Obs}(X_i)\ \prod_i dX_i\,, \tag{4}$$

which is plotted in Fig. 8. Shown are the results for our four choices of the $d(p,\gamma)^3$He rate. Its mean and standard deviation are given in Table III. Our final combined value for the baryon-to-photon ratio, is therefore

$$\eta = (6.123 \pm 0.039) \times 10^{-10} \qquad \omega_{\rm b} = 0.02237 \pm 0.00014\,. \tag{5}$$

Also given in the table is the value of η_{10} at the peak of the likelihood distribution which in these cases equals the mean.

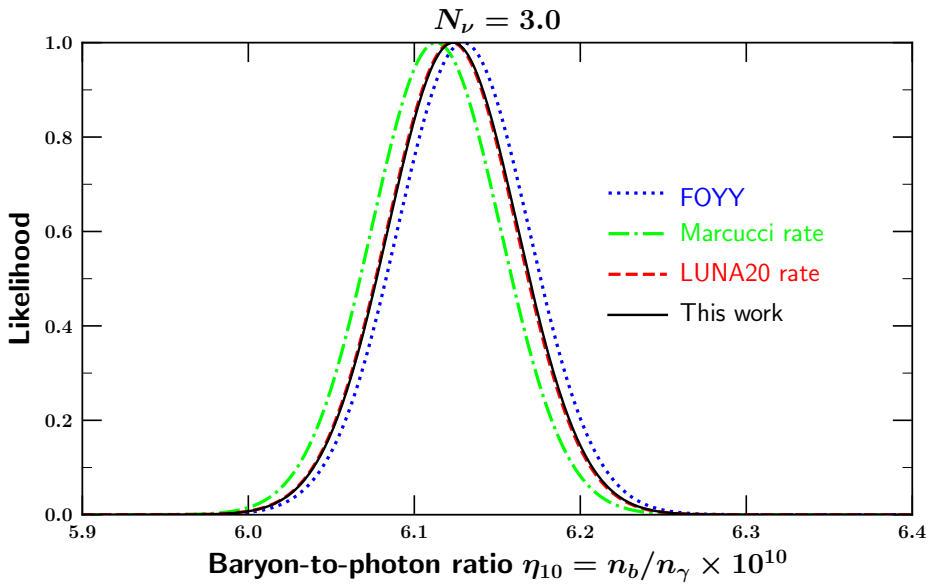


FIG. 8. Baryon-to-photon ratio determinations using the likelihood function defined in Eq. (4) for the four choices of the $d(p,\gamma)^3$He rate considered.

TABLE III. Constraints on the baryon-to-photon ratio, using four choices for the $d(p,\gamma)^3$He rate. We have marginalized over Y_p to create 1D η likelihood distributions. Given are both the mean (and its uncertainty) as well as the value of η at the peak of the distribution.

$d(p,\gamma)^3$He rate	mean η_{10}	peak η_{10}
FOYY [19]	6.129 ± 0.040	6.129
Theory [43]	6.113 ± 0.039	6.113
LUNA20 [47]	6.123 ± 0.039	6.123
This Work	6.123 ± 0.039	6.123

IV. RESULTS FOR VARIABLE N_ν

We turn now to the effect of the new $d(p,\gamma)^3$He rate when we allow N_ν to differ from its Standard Model value of 3. We can repeat the above analysis substituting $\mathcal{L}_{\rm NCMB}(\eta, Y_p, N_\nu)$

for $\mathcal{L}_{\rm CMB}(\eta, Y_p)$ and $\mathcal{L}_{\rm NBBN}(\eta, N_\nu; X_i)$ for $\mathcal{L}_{\rm BBN}(\eta; X_i)$. Integrating these generalized likelihood functions over η as in Eq. (3), we obtain the likelihood distributions for D/H shown in Fig. 9 for our four choices of $d(p,\gamma)^3$He rates. As we would expect, the higher $d(p,\gamma)^3$He rates (relative to the one used in FOYY) causes the BBN likelihood function for D/H (shown in purple) to shift to the left (towards smaller values of D/H). In fact, when N_ν is not fixed, the shift to lower D/H is greater than we saw in Fig. 3, for reasons which will become clear below.

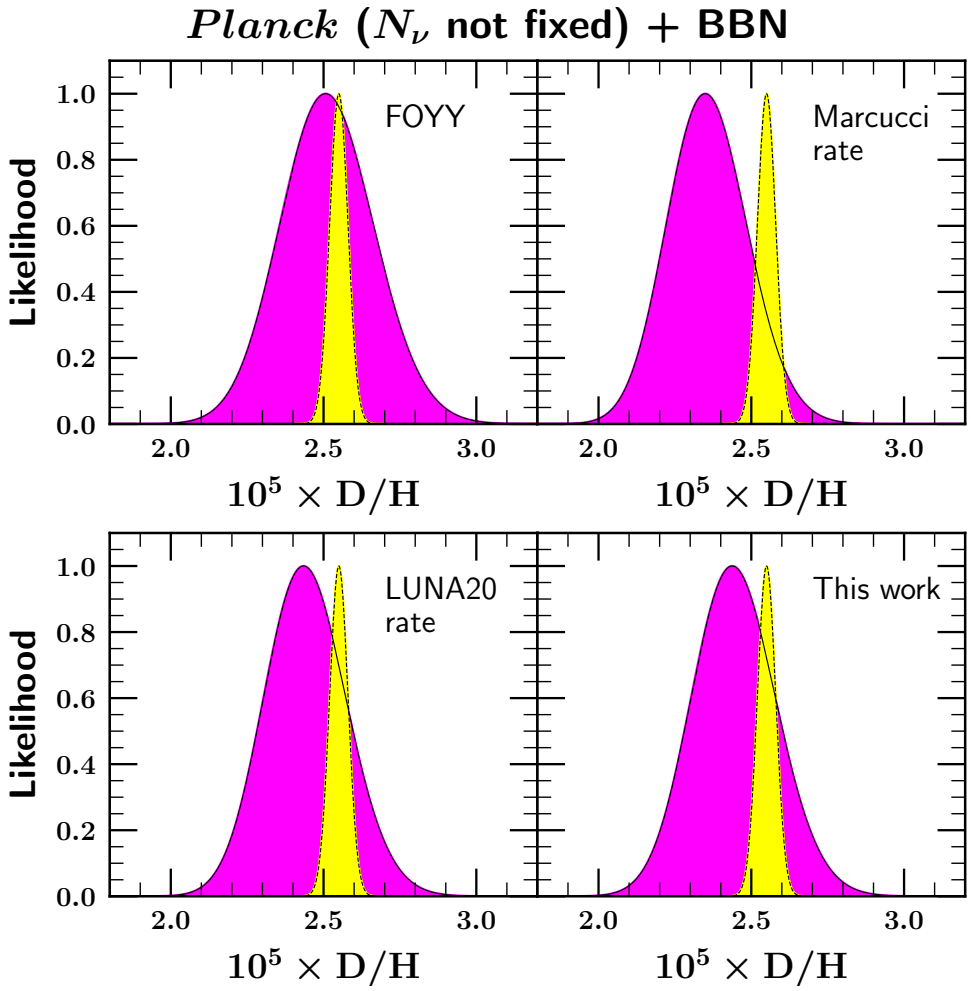


FIG. 9. As in Fig. 3, the predictions for D/H using the CMB determination of the cosmic baryon density when N_ν is not fixed.

The BBN+CMB likelihoods in Fig. 9 are summarized by the predicted abundances for D/H given in Table IV where again the central values give the mean, and the error gives

the 1σ variance and the final column gives the value at the peak of the distribution shown in the purple shaded distributions in Fig. 9. For completeness, we also provide in Table V, the ^{4}He and ^{7}Li abundances for each case.

TABLE IV. The mean and peak values of D/H for each of the adopted rates for $d(p,\gamma)^3$He when N_ν is not held fixed.

$d(p,\gamma)^3$He rate	mean D/H $\times 10^5$	peak D/H $\times 10^5$
FOYY [19]	2.514 ± 0.152	2.506
Theory [43]	2.359 ± 0.131	2.349
LUNA20 [47]	2.444 ± 0.133	2.434
This Work	2.447 ± 0.137	2.437

TABLE V. The mean and peak values of Y_p and Li/H for each of the adopted rates for $d(p,\gamma)^3$He when N_ν is not held fixed.

$d(p,\gamma)^3$He rate	mean Y_p	peak Y_p
FOYY [19]	0.24408 ± 0.00407	0.24440
Theory [43]	0.24409 ± 0.00408	0.24441
LUNA20 [47]	0.24408 ± 0.00408	0.24441
This Work	0.24408 ± 0.00408	0.24441
$d(p,\gamma)^3$He rate	mean Li/H $\times 10^{10}$	peak Li/H $\times 10^{10}$
FOYY [19]	4.78 ± 0.74	4.78
Theory [43]	5.34 ± 0.77	5.33
LUNA20 [47]	5.02 ± 0.72	5.00
This Work	5.01 ± 0.73	5.00

In this case, we can obtain 1-dimensional likelihood functions by integrating with respect to N_ν or η given by

$$\mathcal{L}_{\rm NBBN+NCMB+Obs}(\eta) \propto \int \mathcal{L}_{\rm NCMB}(\eta, Y_p, N_\nu)\mathcal{L}_{\rm NBBN}(\eta, N_\nu; X_i)\ \mathcal{L}_{\rm Obs}(X_i)\ \prod_i dX_i dN_\nu\,, \quad (6)$$

or

$$\mathcal{L}_{\rm NBBN+NCMB+Obs}(N_\nu) \propto \int \mathcal{L}_{\rm NCMB}(\eta, N_\nu, Y_p)\mathcal{L}_{\rm NBBN}(\eta, N_\nu; X_i)\ \mathcal{L}_{\rm Obs}(X_i)\ \prod_i dX_i d\eta\,. \quad (7)$$

These are shown in the left and right panels of Fig. 10 respectively. Almost independent of the $d(p,\gamma)^3$He rate, we see that the best fit solution for η_{10} is lower and we find $\eta_{10} = 6.092 \pm 0.054$. The mean, width, and peak of each of these likelihood functions are summarized in Table VI. Also included in this table is the result based the FOYY rate, but with an updated value for Y_p from [29]. While the value of η is only marginally increased by the updated Y_p, the mean value of N_ν is increased and its uncertainty is decreased. The new value of Y_p is used in all subsequent results shown. This shift downwards in η is predominantly due to the CMB likelihood as discussed in FOYY. Similarly, the most likely values for N_ν are also slightly below 3.0. Using the new rate for $d(p,\gamma)^3$He , when BBN and CMB and observations are combined we find

$$N_\nu = 2.880 \pm 0.144 \tag{8}$$

giving 68% and 95% confidence level upper limits to $N_\nu - 3$ of 0.024 and 0.168 respectively.

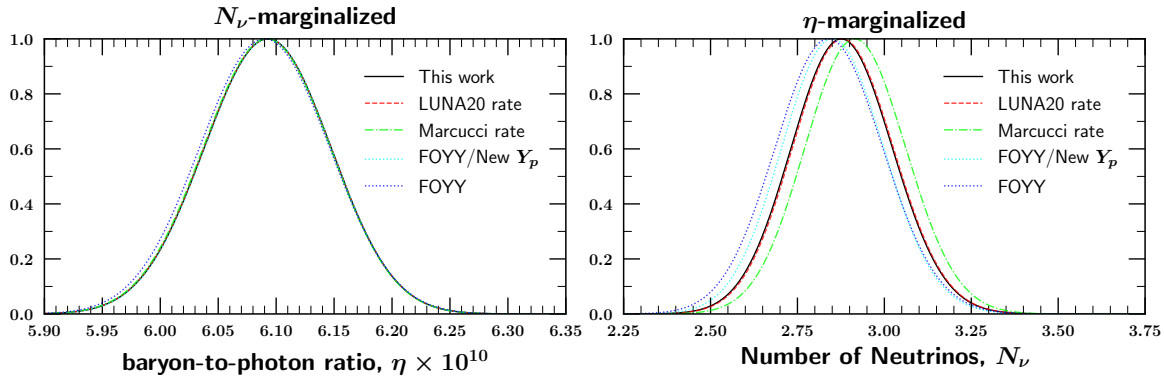


FIG. 10. (Left) As in Fig. 8, but where N_ν is allowed to vary, and results marginalized over it. (Right) The likelihood as a function of N_ν, which is marginalized over η.

These results allow us to understand the downward shift in D/H seen in Fig. 9. While, the lower value of η (6.09 relative to 6.12) produces a 0.8% increase in D/H, this is over-compensated by a 1.6% shift down in D/H due to the lower value in N_ν, since D/H scales as $N_\nu^{0.405}$ as given in the appendix.

V. SUMMARY

Predictions from BBN are limited by the precision of the nuclear rates used in BBN calculations. As such, the new rates for $d(p,\gamma)^3$He provided by the LUNA collaboration are

TABLE VI. The marginalized most-likely values and central 68.3% confidence limits on the baryon-to-photon ratio and effective number of neutrinos, for each choice of the $d(p,\gamma)^3$He rate.

$d(p,\gamma)^3$He rate	mean η_{10}	peak η_{10}	mean N_ν	peak N_ν
FOYY [19]	6.090 ± 0.055	6.090	2.843 ± 0.154	2.839
updated Y_P [19, 29]	6.093 ± 0.054	6.093	2.855 ± 0.146	2.851
Theory [43]	6.092 ± 0.054	6.092	2.918 ± 0.144	2.915
LUNA20 [47]	6.092 ± 0.054	6.093	2.883 ± 0.144	2.879
This Work	6.092 ± 0.054	6.093	2.880 ± 0.144	2.876

indeed welcome. In addition to providing a higher degree of accuracy, they also help resolve the discrepancy between older experimental rates, and theoretical calculations, suggesting that more work on the theory is needed to explain the new rates.

The new rates reaffirm the excellent agreement between BBN/CMB calculated light element abundances, and their observational determinations. At the fixed value of η as determined in this work and shown in the last line of Table III, we compare our results with previous results.

TABLE VII. Comparison of BBN Results

	η_{10}	N_ν	Y_p	D/H	^{3}He/H	^{7}Li/H
Ref. [18]	6.10	3	0.2470	2.579×10^{-5}	0.9996×10^{-5}	4.648×10^{-10}
Ref. [17]	6.091	3	0.2471	2.459×10^{-5}	1.074×10^{-5}	5.624×10^{-10}
Ref. [19]	6.129	3	0.2470	2.559×10^{-5}	0.9965×10^{-5}	4.702×10^{-10}
This Work	6.123	3	0.2470	2.493×10^{-5}	1.033×10^{-5}	4.926×10^{-10}

Table VII compares our results with those of earlier work. The values quoted are not from a full Monte Carlo analysis but rather results for a single value of η, and the reaction rates at their central value. The abundance differences are the result of different nuclear rates. Our new D/H abundance is lower than our earlier results in FOYY [19] and in ref. [18] due to the increased destruction via $d(p,\gamma)^3$He . While it appears that our new result for D/H is closer to that of the Paris group [17], these are evaluated at different values of η. At the same value of η our D/H remains significantly higher, as the $d(p,\gamma)^3$He rate employed in [17]

lies above the LUNA data. Finally, we see that for the same η our Y_p and ^{3}He abundances are quite similar due to their weak dependence on this rate.

Fig. 11 summarizes our results with a Schramm plot on our newly averaged $d(p,\gamma)^3$He rate. The thickness of each curve depicts the $\pm 1\sigma$ spread in the predicted abundances. The relative uncertainty, (the thickness of the curves, relative to the central value) is shown more clearly in Figure 12. As one can see, the ^{7}Li abundance remains the most uncertain, with a relative uncertainty of approximately 13%. The uncertainty in the deuterium abundance ranges from 3.5-5%, while the calculated uncertainty in ^{4}He is only 0.1% (note that it is amplified by a factor of 10 in the figure for clarity). Comparison with the FOYY results shown by the dotted curves confirms the substantial improvement due to the LUNA measurements.

As we have seen, the uncertainty in the BBN prediction of D/H has decreased, yet still falls short of the precision of the observations. It is thus important to re-evaluate the error budget for primordial deuterium. As seen in the Appendix, in addition to $d(p,\gamma)^3$He , deuterium has strong sensitivity to the $d(d,n)^3$He and $d(d,p)t$ rates. To quantify this effect, we have run a Monte Carlo calculation at fixed $\eta_{10} = 6.123$ to evaluate the contribution $\sigma_i(D/H)$ to the D/H uncertainty from individual reactions i with all other rate uncertainties set to zero; these are shown in the second column of Table VIII. In the third column of Table VIII, we show the D/H uncertainty when *only* the contribution from reaction i is set to zero, denoted $\sigma_{\mathrm{omit}\ i}$(D/H). One can verify that the total uncertainty very closely follows the simple error propagation result for the sum of uncorrelated random variables: $\sigma^2_{\mathrm{tot}} = \sum_i \sigma_i^2$. Similarly, $\sigma^2_{\mathrm{tot}} = \sigma_i^2 + \sigma^2_{\mathrm{omit}\ i}$ to an excellent approximation.

Table VIII summarizes the new landscape of D/H nuclear uncertainties and points the way to future progress. We see that $d(p,\gamma)^3$He is now well under control: it barely contributes to the total D/H error. Indeed, even letting the uncertainty go to zero would barely improve the final D/H precision. This is a testament to the power of the LUNA result. Thus, further improvement in D/H turns to other reactions. In particular, $d(d,n)^3$He now clearly dominates the error budget, with $d(d,p)t$ in somewhat distant second place. Fortunately, both reactions have the same initial state, and so both can be accessible in the same experiment. From the table we see that a factor of ~ 2 improvement in uncertainty would bring the $d(d,n)$ contribution to σ(D/H) down the level of the new $d(p,\gamma)^3$He results.

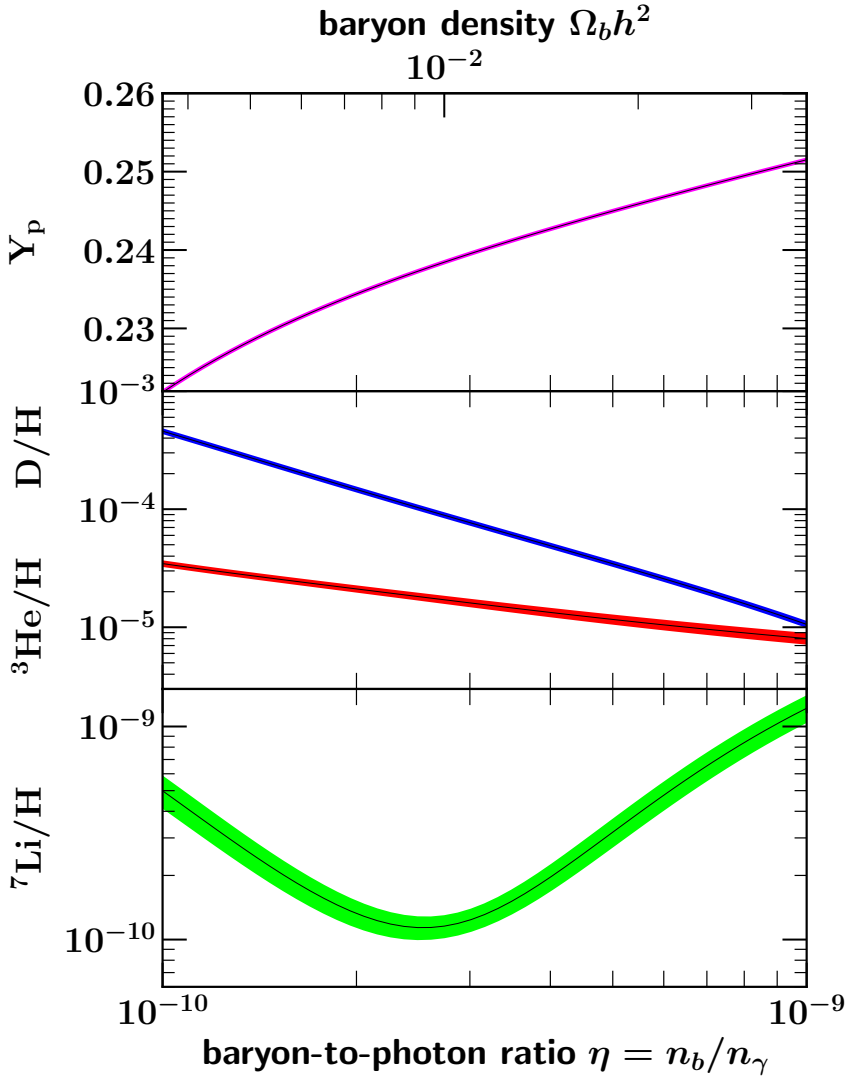


FIG. 11. Primordial abundances of the light nuclides as a function of cosmic baryon content, as predicted by SBBN ("Schramm plot"). These results assume $N_\nu = 3$ and the current measurement of the neutron lifetime $\tau_n = 879.4 \pm 0.6$ s. Curve widths show 1σ errors.

We have thus seen that the new LUNA measurements have substantially improved the experimental underpinnings of primordial deuterium production. The $d(p,\gamma)^3$He rate is now well-determined in the BBN energy range, and contributes small part of the D/H error budget. The D/H theory prediction is now significantly sharper, though it has still has not caught up to observational precision. These improvements are important for both standard and non-standard BBN. For standard BBN, the constraints on the baryon density tighten

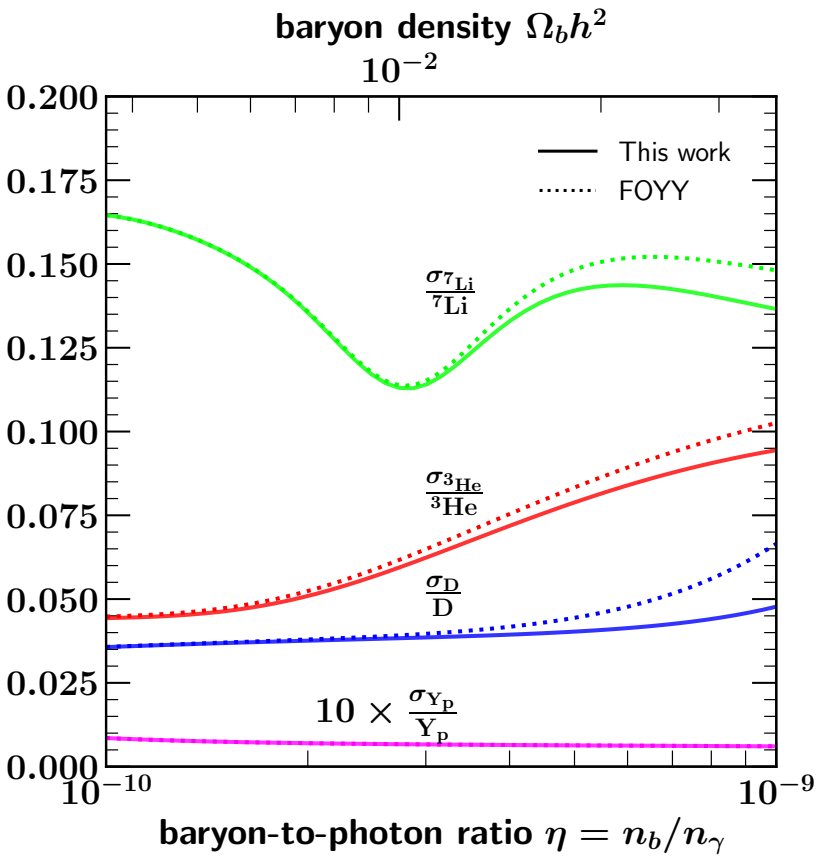


FIG. 12. Fractional uncertainties in the light element abundance predictions shown in Fig. 11. For each species i, we plot ratio of the standard deviation σ_i to the mean μ_i, as a function of baryon-to-photon ratio. The relative uncertainty of the ^{4}He abundance has been multiplied by a factor of 10.

and thus afford a sharper comparison with CMB. For NBBN, we find notably stronger bounds on N_ν.

Future work can capitalize on these improvements and push for further precision. Because the BBN+CMB prediction errors still lag the observations, we urge new, precise measurements of the $d(d,n)$ and $d(d,p)$ reactions in the BBN energy range. The planned next generation CMB-Stage IV experiment [58] should substantially improve the CMB determination of N_ν and Y_p, increasing the power of the comparison with BBN and possibly detecting the $N_{\rm eff} - N_\nu = 0.045$ difference, thus probing effects of neutrino heating during $e^\pm$ annihilation. Finally, of course the lithium problem continues to awaits a firm solution.

Note added: As this paper was in the final stages of preparation, we became aware of two

TABLE VIII. Deuterium Uncertainty Contributions at $\eta_{10} = 6.123$

Reaction i	$10^5\ \sigma_i$(D/H)	$10^5\ \sigma_{\mathrm{omit}\ i}$(D/H)
$d(p,\gamma)^3$He	0.036	0.097
$d(d,n)^3$He	0.081	0.065
$d(d,p)t$	0.054	0.089
^{3}He$(d,p)^4$He	0.002	0.103
$p(n,\gamma)d$	0.002	0.103
^{3}He$(n,p)t$	0.002	0.103
all	0.103	–

works similar to our own. Ref. [59] builds on their work with LUNA [47], coming to similar conclusions as ours for SBBN and NBBN. In Ref. [60], the Paris group performs their own analysis of the impact of the LUNA measurements on Standard BBN with $N_\nu = 3$. Their nuclear rates make use of theory, including for $d(p,\gamma)^3$He , giving a deuterium abundance $(\mathrm{D/H})_{\mathrm{BBN+CMB}} = (2.439 \pm 0.037) \times 10^{-5}$. This is substantially lower than both our result and the observations, and consequences of this mismatch are discussed. That these conclusions are so different emphasizes the continuing central role of nuclear reactions and their analysis for BBN.

APPENDIX

In this appendix, we update the fractional dependence of the light element abundances to η, N_ν, the gravitational constant, the neutron mean life, and a selection of nuclear rates. For each element we give

$$X_i = X_{i,0} \prod_n \left(\frac{p_n}{p_{n,0}} \right)^{\alpha_n} , \tag{9}$$

where X_i represents either the helium mass fraction or the abundances of the other light elements by number. The p_n represent input quantities to the BBN calculations, whose power-law scaling is the log derivative $\alpha_i = \partial \ln X_i / \partial \ln p_i$. Below are the scalings with these inputs, as defined in detail in FOYY and ref. [18].

$$\begin{aligned} Y_p = 0.24695 &\left(\frac{\eta_{10}}{6.123} \right)^{0.039} \left(\frac{N_\nu}{3.0} \right)^{0.163} \left(\frac{G_N}{G_{N,0}} \right)^{0.357} \left(\frac{\tau_n}{879.4s} \right)^{0.729} \\ &\times \left[p(n,\gamma)d \right]^{0.005} \left[d(d,n)^3\mathrm{He} \right]^{0.006} \left[d(d,p)t \right]^{0.005} \end{aligned} \tag{10}$$

$$\frac{\mathrm{D}}{\mathrm{H}} = 2.493\times10^{-5}\left(\frac{\eta_{10}}{6.123}\right)^{-1.634}\left(\frac{N_\nu}{3.0}\right)^{0.405}\left(\frac{G_N}{G_{N,0}}\right)^{0.974}\left(\frac{\tau_n}{879.4s}\right)^{0.418}$$
$$\times\,[p(n,\gamma)d]^{-0.197}\,[d(d,n)^3\mathrm{He}]^{-0.529}\,[d(d,p)t]^{-0.468}$$
$$\times\,[d(p,\gamma)^3\mathrm{He}]^{-0.344}\,[^3\mathrm{He}(n,p)t]^{0.024}\,[^3\mathrm{He}(d,p)^4\mathrm{He}]^{-0.014} \qquad (11)$$

$$\frac{^3\mathrm{He}}{\mathrm{H}} = 1.033\times10^{-5}\left(\frac{\eta_{10}}{6.123}\right)^{-0.564}\left(\frac{N_\nu}{3.0}\right)^{0.135}\left(\frac{G_N}{G_{N,0}}\right)^{0.324}\left(\frac{\tau_n}{879.4s}\right)^{0.139}$$
$$\times\,[p(n,\gamma)d]^{0.087}\,[d(d,n)^3\mathrm{He}]^{0.198}\,[d(d,p)t]^{-0.257}$$
$$\times\,[d(p,\gamma)^3\mathrm{He}]^{0.395}\,[^3\mathrm{He}(n,p)t]^{-0.166}\,[^3\mathrm{He}(d,p)^4\mathrm{He}]^{-0.759}\,[t(d,n)^4\mathrm{He}]^{-0.008} \qquad (12)$$

$$\frac{^7\mathrm{Li}}{\mathrm{H}} = 4.926\times10^{-10}\left(\frac{\eta_{10}}{6.123}\right)^{2.118}\left(\frac{N_\nu}{3.0}\right)^{-0.286}\left(\frac{G_N}{G_{N,0}}\right)^{-0.732}\left(\frac{\tau_n}{879.4s}\right)^{0.429}$$
$$\times\,[p(n,\gamma)d]^{1.308}\,[d(d,n)^3\mathrm{He}]^{0.677}\,[d(d,p)t]^{0.062}$$
$$\times\,[d(p,\gamma)^3\mathrm{He}]^{0.623}\,[^3\mathrm{He}(n,p)t]^{-0.266}\,[^3\mathrm{He}(d,p)^4\mathrm{He}]^{-0.750}\,[t(d,n)^4\mathrm{He}]^{-0.021}$$
$$\times\,[^3\mathrm{He}(\alpha,\gamma)^7\mathrm{Be}]^{0.965}\,[^7\mathrm{Be}(n,p)^7\mathrm{Li}]^{-0.692}\,[^7\mathrm{Li}(p,\alpha)^4\mathrm{He}]^{-0.052}\,[t(\alpha,\gamma)^7\mathrm{Li}]^{0.027}$$
$$\times\,[^7\mathrm{Be}(n,\alpha)^4\mathrm{He}]^{-0.001}\,[^7\mathrm{Be}(d,p)^4\mathrm{He}^4\mathrm{He}]^{-0.008} \qquad (13)$$

ACKNOWLEDGMENTS

The work of K.A.O. was supported in part by DOE grant DE-SC0011842 at the University of Minnesota.

---

[1] T. P. Walker, G. Steigman, D. N. Schramm, K. A. Olive and H. S. Kang, Astrophys. J. **376** (1991) 51; K. A. Olive, G. Steigman and T. P. Walker, Phys. Rept. **333**, 389 (2000) [astro-ph/9905320]; B. D. Fields and K. A. Olive, Nucl. Phys. **A777**, 208 (2006); B. D. Fields, P. Molaro and S. Sarkar, Chin. Phys. C **38** (2014) [arXiv:1412.1408 [astro-ph.CO]]; G. Steigman, Ann. Rev. Nucl. Part. Sci. **57**, 463 (2007) [arXiv:0712.1100 [astro-ph]].

[2] R. H. Cyburt, B. D. Fields and K. A. Olive, *New Astron.* **6** (1996) 215 [arXiv:astro-ph/0102179].

[3] K. M. Nollett and S. Burles, Phys. Rev. D **61**, 123505 (2000) [astro-ph/0001440]; S. Burles, K. M. Nollett and M. S. Turner, Astrophys. J. **552**, L1 (2001) [astro-ph/0010171].

[4] E. Vangioni-Flam, A. Coc and M. Casse, Astron. Astrophys. **360**, 15 (2000) [astro-ph/0002248];

[5] R. H. Cyburt, B. D. Fields and K. A. Olive, Astropart. Phys. **17** (2002) 87 [arXiv:astro-ph/0105397].

[6] R. H. Cyburt, B. D. Fields and K. A. Olive, Phys. Lett. B **567**, 227 (2003) [astro-ph/0302431].

[7] A. Coc, E. Vangioni-Flam, P. Descouvemont, A. Adahchour and C. Angulo, *Ap. J.* **600** (2004) 544 [arXiv:astro-ph/0309480].

[8] A. Cuoco, F. Iocco, G. Mangano, G. Miele, O. Pisanti and P. D. Serpico, Int. J. Mod. Phys. A **19** (2004) 4431 [arXiv:astro-ph/0307213]; P. D. Serpico, S. Esposito, F. Iocco, G. Mangano, G. Miele and O. Pisanti, JCAP **0412**, 010 (2004) [arXiv:astro-ph/0408076];

[9] R. H. Cyburt, Phys. Rev. D **70** (2004) 023505 [arXiv:astro-ph/0401091].

[10] P. Descouvemont, A. Adahchour, C. Angulo, A. Coc and E. Vangioni-Flam, ADNDT **88** (2004) 203 [arXiv:astro-ph/0407101];

[11] F. Iocco, G. Mangano, G. Miele, O. Pisanti and P. D. Serpico, Phys. Rept. **472**, 1 (2009) [arXiv:0809.0631 [astro-ph]].

[12] O. Pisanti, A. Cirillo, S. Esposito, F. Iocco, G. Mangano, G. Miele and P. D. Serpico, Comput. Phys. Commun. **178**, 956 (2008) [arXiv:0705.0290 [astro-ph]].

[13] A. Coc, S. Goriely, Y. Xu, M. Saimpert and E. Vangioni, Astrophys. J. **744**, 158 (2012) [arXiv:1107.1117 [astro-ph.CO]].

[14] R. H. Cyburt, B. D. Fields and K. A. Olive, JCAP **0811**, 012 (2008) [arXiv:0808.2818 [astro-ph]].

[15] A. Coc, J. P. Uzan and E. Vangioni, JCAP **1410**, 050 (2014) [arXiv:1403.6694 [astro-ph.CO]].

[16] A. Coc, P. Petitjean, J. P. Uzan, E. Vangioni, P. Descouvemont, C. Iliadis and R. Longland, Phys. Rev. D **92**, no. 12, 123526 (2015) [arXiv:1511.03843 [astro-ph.CO]].

[17] C. Pitrou, A. Coc, J. P. Uzan and E. Vangioni, Phys. Rept. **754**, 1 (2018) [arXiv:1801.08023 [astro-ph.CO]].

[18] R. H. Cyburt, B. D. Fields, K. A. Olive and T.-H. Yeh, Rev. Mod. Phys. **88**, 015004 (2016) [arXiv:1505.01076 [astro-ph.CO]].

[19] B. D. Fields, K. A. Olive, T. H. Yeh and C. Young, JCAP **03**, 010 (2020) [arXiv:1912.01132 [astro-ph.CO]].

[20] P. A. Zyla *et al.* [Particle Data Group], PTEP **2020**, no.8, 083C01 (2020)

[21] N. Aghanim *et al.* [Planck Collaboration], Astron. Astrophys. **641** (2020), A6 [arXiv:1807.06209 [astro-ph.CO]].

[22] R. H. Cyburt, B. D. Fields and K. A. Olive, Phys. Rev. D **69**, 123519 (2004) [arXiv:astro-ph/0312629].

[23] R. N. Boyd, C. R. Brune, G. M. Fuller and C. J. Smith, Phys. Rev. D **82**, 105005 (2010) [arXiv:1008.0848 [astro-ph.CO]].

[24] C. Broggini, L. Canton, G. Fiorentini and F. L. Villante, JCAP **1206**, 030 (2012) [arXiv:1202.5232 [astro-ph.CO]].

[25] C. Iliadis and A. Coc, Astrophys. J. **901** (2020) no.2, 127 [arXiv:2008.12200 [astro-ph.CO]].

[26] S. Vauclair,and C. Charbonnel, Ap. J. **502** (1998) 372 [arXiv:astro-ph/9802315]; M. H. Pinsonneault, T. P. Walker, G. Steigman and V. K. Narayanan, Ap. J. **527** (1998) 180 [arXiv:astro-ph/9803073]; M. H. Pinsonneault, G. Steigman, T. P. Walker, and V. K. Narayanan, Ap. J. **574** (2002) 398 [arXiv:astro-ph/0105439]; O. Richard, G. Michaud and J. Richer, Astrophys. J. **619**, 538 (2005) [arXiv:astro-ph/0409672]; A. J. Korn *et al.*, Nature **442**, 657 (2006) [arXiv:astro-ph/0608201]; A. E. García Peréz, S., Inoue, W. Aoki, and S. G. Ryan, in Precision Spectroscopy in Astrophysics, Proceedings of the ESO/Lisbon/Aveiro Conference, 9 (2008).

[27] L. Sbordone, P. Bonifacio, E. Caffau, H.-G. Ludwig, N. T. Behara, J. I. G. Hernandez, M. Steffen and R. Cayrel *et al.*, Astron. Astrophys. **522**, A26 (2010) [arXiv:1003.4510 [astro-ph.GA]]; P. Bonifacio, E. Caffau, M. Spite, F. Spite, L. Sbordone, L. Monaco, P. François, B. Plez, P. Molaro and A. J. Gallagher, *et al.* Astron. Astrophys. **612**, A65 (2018) [arXiv:1801.03935 [astro-ph.SR]]; D. S. Aguado, J. I. G. Hernández, C. Allende Prieto and R. Rebolo, Astrophys. J. Lett. **874**, L21 (2019) [arXiv:1904.04892 [astro-ph.SR]]; J.D. Simpson *et al.* [arXiv:2011.02659 [astro-ph.GA]].

[28] B. D. Fields, Ann. Rev. Nucl. Part. Sci. **61**, 47 (2011) [arXiv:1203.3551 [astro-ph.CO]].

[29] E. Aver, D. A. Berg, K. A. Olive, R. W. Pogge, J. J. Salzer and E. D. Skillman, [arXiv:2010.04180 [astro-ph.CO]].

[30] E. Aver, K. A. Olive and E. D. Skillman, JCAP **1507**, no. 07, 011 (2015) [arXiv:1503.08146 [astro-ph.CO]].

[31] M. Pettini and R. Cooke, Mon. Not. Roy. Astron. Soc. **425**, 2477 (2012) [arXiv:1205.3785 [astro-ph.CO]].

[32] R. Cooke, M. Pettini, R. A. Jorgenson, M. T. Murphy and C. C. Steidel, Ap. J. **781**, 31 (2014) [arXiv:1308.3240 [astro-ph.CO]].

[33] S. Riemer-Sørensen *et al.*, Mon. Not. Roy. Astron. Soc. **447**, 2925 (2015) [arXiv:1412.4043 [astro-ph.CO]].

[34] S. A. Balashev, E. O. Zavarygin, A. V. Ivanchik, K. N. Telikova and D. A. Varshalovich, Mon. Not. Roy. Astron. Soc. **458**, no. 2, 2188 (2016) [arXiv:1511.01797 [astro-ph.GA]].

[35] R. J. Cooke, M. Pettini, K. M. Nollett and R. Jorgenson, Astrophys. J. **830**, no. 2, 148 (2016) [arXiv:1607.03900 [astro-ph.CO]].

[36] S. Riemer-Sørensen, S. Kotuš, J. K. Webb, K. Ali, V. Dumont, M. T. Murphy and R. F. Carswell, Mon. Not. Roy. Astron. Soc. **468**, no. 3, 3239 (2017) [arXiv:1703.06656 [astro-ph.CO]].

[37] E. O. Zavarygin, J. K. Webb, V. Dumont, S. Riemer-Sørensen, Mon. Not. Roy. Astron. Soc. **477**, no. 4, 5536 (2018) [arXiv:1706.09512 [astro-ph.GA]].

[38] R. J. Cooke, M. Pettini and C. C. Steidel, Astrophys. J. **855**, no. 2, 102 (2018) [arXiv:1710.11129 [astro-ph.CO]].

[39] Y. Xu, K. Takahashi, S. Goriely, M. Arnould, M. Ohta and H. Utsunomiya, Nucl. Phys. A **918**, 61 (2013) [arXiv:1310.7099 [nucl-th]].

[40] Nollett K. M. and G. P. Holder, 2011 arXiv:1112.2683 [astro-ph.CO].

[41] Burles S., K. M. Nollett, J. W. Truran and M. S. Turner, 1999, Phys. Rev. Lett. **82**, 4176 [astro-ph/9901157].

[42] L. E. Marcucci, M. Viviani, R. Schiavilla, A. Kievsky and S. Rosati, Phys. Rev. C **72**, 014001 (2005) [nucl-th/0502048].

[43] L. E. Marcucci, G. Mangano, A. Kievsky and M. Viviani, Phys. Rev. Lett. **116**, no. 10, 102501 (2016) Erratum: [Phys. Rev. Lett. **117**, no. 4, 049901 (2016)] [arXiv:1510.07877 [nucl-th]].

[44] I. Tišma, M. Lipoglavšek, M. Mihovilovič, S. Markelj, M. Vencelj and J. Vesić, Eur. Phys. J. A **55**, no.8, 137 (2019)

[45] D. Trezzi *et al.* [LUNA Collaboration], J. Phys. Conf. Ser. **940**, no. 1, 012059 (2018).

[46] V. Mossa, K. Stöckel, F. Cavanna, F. Ferraro, M. Aliotta, F. Barile, D. Bemmerer, A. Best, A. Boeltzig and C. Broggini, *et al.* Eur. Phys. J. A **56**, no.5, 144 (2020) [arXiv:2005.00002 [physics.ins-det]].

[47] V. Mossa, K. Stöckel, F. Cavanna, F. Ferraro, M. Aliotta, F. Barile, D. Bemmerer, A. Best, A. Boeltzig and C. Broggini, *et al.* Nature **587**, 210 (2020).

[48] G. J. Schmid, B. J. Rice, R. M. Chasteler, M. A. Godwin, G. C. Kiang, L. L. Kiang, C. M. Laymon, R. M. Prior, D. R. Tilley and H. R. Weller, Phys. Rev. C **56**, 2565-2581 (1997)

[49] L. Ma, H. J. Karwowski, C. R. Brune, Z. Ayer, T. C. Black, J. C. Blackmon, E. J. Ludwig, M. Viviani, A. Kievsky and R. Schiavilla, Phys. Rev. C **55**, 588-596 (1997)

[50] W. Wölfli, R. Bosch, J. Lang, R. Muller, P. Helv. Phys. Acta **40**, 946 (1967).

[51] Griffiths, G.M., Larson, E.A., and Robertson, L.P.: 1962, *Canadian Journal of Physics* **40**, 402.

[52] Bailey, G.M., Griffiths, G.M., Olivo, M.A., and Helmer, R.L.: 1970, *Canadian Journal of Physics* **48**, 3059.

[53] Griffiths, G.M., Lal, M., and Scarfe, C.D.: 1963, *Canadian Journal of Physics* **41**, 724.

[54] L. M. Krauss and P. Romanelli, Astrophys. J. **358**, 47 (1990); M. S. Smith, L. H. Kawano and R. A. Malaney, Astrophys. J. Suppl. **85**, 219 (1993).

[55] P. J. Kernan and L. M. Krauss, Phys. Rev. Lett. **72**, 3309 (1994) [astro-ph/9402010]; L. M. Krauss and P. J. Kernan, Phys. Lett. B **347**, 347 (1995) [astro-ph/9408023].

[56] N. Hata, R. J. Scherrer, G. Steigman, D. Thomas and T. P. Walker, Astrophys. J. **458**, 637 (1996) [astro-ph/9412087].

[57] B. D. Fields and K. A. Olive, Phys. Lett. B **368**, 103 (1996) [hep-ph/9508344]; B. D. Fields, K. Kainulainen, K. A. Olive and D. Thomas, New Astron. **1**, 77 (1996) [astro-ph/9603009].

[58] K. Abazajian *et al.*, arXiv:1907.04473 [astro-ph.IM].

[59] O. Pisanti, G. Mangano, G. Miele and P. Mazzella, [arXiv:2011.11537 [astro-ph.CO]].

[60] C. Pitrou, A. Coc, J. P. Uzan and E. Vangioni, [arXiv:2011.11320 [astro-ph.CO]].